Applied Surface Science 538 (2021) 148029

Contents lists available at ScienceDirect

Applied Surface Science

journal homepage: www.elsevier.com/locate/apsusc

Preparation of titania-reduced graphene oxide composite coatings with electro- and photosensitive properties

Lucas M.C. Silva[a], Bruno S. Gonçalves[a], Jorgimara de O. Braga[a], Tarcizo C. de Souza[b,c], Vinícius G. de Castro[c], Glaura G. Silva[c,d], Glenda R.B.S. Lacerda[d], Tulio Matencio[b,d], Tiago C. Barbosa[c], Carlos M. Viana[c], Manuel Houmard[b], Eduardo H.M. Nunes[a,*]

[a] Departamento de Engenharia Metalúrgica e de Materiais, Universidade Federal de Minas Gerais, Escola de Engenharia, Bloco 2, Sala 2233, Pampulha, CEP: 31270-901 Belo Horizonte, MG, Brazil
[b] Departamento de Engenharia Química, Universidade Federal de Minas Gerais, Escola de Engenharia, Bloco 2, Sala 5210, Pampulha, CEP: 31270-901 Belo Horizonte, MG, Brazil
[c] Centro de Tecnologia em Nanomateriais e Grafeno (CTNano-UFMG), Rua Professor José Vieira de Mendonça, 1000 - Engenho Nogueira, CEP: 31310-260 Belo Horizonte, MG, Brazil
[d] Departamento de Química, Universidade Federal de Minas Gerais, Instituto de Ciências Exatas, Pampulha, CEP: 31270-901 Belo Horizonte, MG, Brazil

ARTICLE INFO

Keywords:
Titania
Graphene oxide
Wettability
UV illumination
Calcination
Electrical properties

ABSTRACT

Smooth and optically transparent titania (TiO_2) and TiO_2-reduced graphene oxide (RGO) composite films were successfully prepared here. A nanocrystalline anatase suspension was initially prepared by combining the sol-gel process and hydrothermal treatment. Graphene oxide (GO) nanosheets were prepared following a route similar to the Hummers method. Glass slides were then dip-coated using mixtures of TiO_2 and GO suspensions. The concentration of GO in the prepared coatings ranged from 1 to 5 wt%. The coated samples were air-dried, and then either calcined or irradiated with UVA light. It was observed that UVA light promoted the reduction of GO to RGO, which increased both the electrical conductivity and hydrophilicity of the composites. The heat treatment of as-prepared coatings also decreased the water contact angle (WCA) with its surface, which is related to the removal of organics residues, graphene burning, and the increase in surface energy. The super-hydrophilicity of the prepared samples was investigated after keeping them in air for up to 60 days, followed by UVA illumination. It was also demonstrated that a hydrophilic behavior can be induced in the samples prepared here by applying a direct current (DC) voltage, which could allow their use as smart materials in several applications.

1. Introduction

Titania (TiO_2) is a semiconductor with relevant environmental and biomedical applications, widely used in the photocatalytic degradation of pollutants [1-3], production of H_2 [4], and fabrication of biosensors [5] and batteries [6,7]. It is well known as a powerful oxidizing agent, displaying low cost, good chemical stability, and nontoxicity [8]. TiO_2 has also been used as a superhydrophilic self-cleaning coating, allowing different substrates such as glass, plastic, tiles, building linings, and wood to eliminate bacteria and grime [9]. Such coatings find important applications in many industrial fields, reducing the use of water and chemicals in addition to contributing to the maintenance of the ecosystem [10].

A superhydrophilic behavior can be induced in TiO_2 by exposing it to ultraviolet (UV) light, which is related to the formation of electron-hole pairs (e^-/h^+). This process is associated with the promotion of electrons from the valence band to the conduction band, leading to the creation of holes in the former band. The photogenerated conduction-band electrons can reduce Ti^{4+} to Ti^{3+}, which may form surface defects at bridging oxygen sites. It has been reported that when these surface-defects are generated, water and oxygen compete with each other to chemically adsorb onto it [11,12]. The wetting behavior of such a surface is related to an equilibrium condition of the adsorption process of water and oxygen [13]. Holes generated by the UV illumination of TiO_2 may give rise to oxygen vacancies. Such defects play a key role in the process of water adsorption on TiO_2 [14]. Oxygen vacancies that did not react with previously-adsorbed water and organic molecules may become trapped in the TiO_2 network [15]. The as-created defects

* Corresponding author.
E-mail addresses: mhoumard@ufmg.br (M. Houmard), eduardo.nunes@demet.ufmg.br (E.H.M. Nunes).

https://doi.org/10.1016/j.apsusc.2020.148029
Received 22 February 2020; Received in revised form 26 September 2020; Accepted 28 September 2020
Available online 02 October 2020
0169-4332/

can increase the affinity of TiO_2 for hydroxyl ions (OH^-) arising from the dissociation of chemisorbed water and the creation of hydrophilic areas [9].

Although hydrophilicity and hydrophobicity correspond to two opposite properties of wettability, the behavior of a surface can be switched between these two states by an external stimulus. It is possible, for instance, to change the wetting behavior of TiO_2 from hydrophobic to superhydrophilic by photo-induction [16,17]. As discussed before, the photogenerated charge carriers play an important role in the superhydrophilic behavior of this material. Nonetheless, it is well established that the light-induced superhydrophilicity of TiO_2 does not persist in the absence of UV light, which limits its application because surfaces may not be permanently exposed to UV radiation such as in indoor environments [18]. This time-dependent loss of superhydrophilicity in the absence of an external stimulus may be associated with the recombination of photogenerated electron-hole pairs and surface exposure to air pollution. Many researchers have already suggested different approaches to overcome this limitation. Although the doping of TiO_2 has shown good results [19-21], the high cost and low availability of the commonly used elements are limiting factors for large-scale production of these materials. TiO_2-SiO_2 composites also showed good results on super hydrophilicity [22]. However, the addition of SiO_2 may impair the photocatalytic behavior of the composite [23]. The association between TiO_2 and graphene is a promising approach [24-26]. This behavior is related to an efficient charge transfer between these materials that occurs during the UV illumination of the composite, which promotes an effective separation of the photogenerated electron-hole pairs and slows down the recombination of these charge carriers. It has also been reported that the combination of TiO_2 and graphene may narrow the bandgap of the former [27]. Moreover, the presence of graphene increases the electrical conductivity of TiO_2 and inhibits the adsorption of pollutants on its surface by an antistatic effect [28]. Liu *et al.* [29] investigated the electrochemical behavior of TiO_2 nanorods loaded in graphene oxide and observed that these materials have an enhanced electrochemical performance, which is another attractive property of this composite.

The control of wettability is essential for the development of smart surfaces, such as smart windows. Although several studies have investigated the photoinduced properties of TiO_2 in recent years, its use, when combined with graphene for the preparation of coatings, has been little explored. We recently reported the preparation by the sol-gel process and hydrothermal treatment of titania/reduced graphene oxide (RGO) composites with an improved photodegradation capacity of organic dyes [30,31]. It was observed that under UVA light such materials give rise to reactive oxygen species with a high ability to degrade pollutants. The promising results reported in the literature for TiO_2/RGO composites, along with the expertise of our research group on the preparation of self-cleaning surfaces by the deposition of sol-gel derived titania [22,23,32,33], were the main motivations for this study. In this work, TiO_2 coatings were prepared by hydrothermal treatment and sol-gel dip-coating. Graphene-containing composite films were also prepared to evaluate the effect of this addition on the structural, electrical, and wetting properties of the composites. UV irradiation and calcination in air were tested to investigate their influence on the properties of the obtained coatings. The samples prepared in this study were examined by several techniques such as X-ray diffraction (XRD), Raman spectroscopy, UV–Vis spectroscopy, scanning electron microscopy (SEM), and atomic force microscopy (AFM). The wetting behavior of the prepared samples was evaluated by measuring the contact angle of deionized water with the substrate as a function of aging time, UV illumination, or direct current (DC) voltage application.

2. Materials and methods

2.1. Synthesis of graphene oxide (go) nanosheets

Graphene oxide (GO) nanosheets were obtained after the ultrasonic exfoliation of graphitic oxide (GrO), as described in detail elsewhere [34]. Briefly, a solution of sulfuric acid (H_2SO_4 / Synth / 98%) and potassium permanganate ($KMnO_4$ / Neon / 99%) was initially prepared under stirring in an ice bath. Graphite powder (CBG Mining) was then added to this solution. The suspension was kept under stirring in a microwave digestion system (Milestone Start D) at 250 W and 70 °C for 10 min. The as-prepared slurry was dispersed in cold deionized water, followed by the addition of hydrogen peroxide (H_2O_2 / Dinâmica / 35 vol%) to remove manganese impurities. The slurry was filtered and the remaining solid (GrO) was continuously washed with deionized Milli-Q water until reaching pH 7. GO was obtained after the ultrasonic exfoliation of GrO in water for 30 min. The as-prepared suspension was then centrifuged at 4000 rpm for 20 min and GO was collected as supernatant. The concentration of GO in the obtained suspension was kept constant at 1.0 g/L. It was observed in a previous study that this procedure gives rise to highly-dispersed GO nanosheets about 0.9 nm thick [30].

2.2. Synthesis of titania

A combination of sol-gel processing and hydrothermal treatment was used to obtain a crystalline TiO_2 suspension. A solution of titanium tetraisopropoxide (TTIP / Aldrich / 97%) and absolute ethyl alcohol (EtOH / Aldrich / ≥ 98%) was initially prepared at room temperature. In another flask, EtOH, hydrochloric acid (HCl / Aldrich / 37%), and deionized Milli-Q water were also mixed. After the homogenization of both solutions, they were mixed under vigorous stirring at room temperature. The as-obtained solution was aged at room temperature for at least three days. The molar ratio of TTIP: EtOH: HCl: H_2O was 1: 35: 0.3: 0.3. Deionized water was then added to the solution for adjusting the molar ratio of H_2O: TTIP to 90: 1. A crystalline suspension was obtained after pouring the previously-prepared sol into a Teflon-lined stainless-steel autoclave and heat-treating it at 180 °C for 6 h. It is well established that this hydrothermal treatment promotes the crystallization of TiO_2 into anatase [35]. After this step, particle agglomerate with a gelatin-like texture immersed in a liquid phase was obtained. An exchange procedure was subsequently conducted to replace the acidic liquid phase with absolute EtOH. The liquid phase of the final suspension should be free of H^+ ions and have a pH close to 7. The suspension was then stirred at room temperature for 30 min and sonicated for 1 h to promote the redispersion of anatase crystallites.

2.3. Production of coatings and powdered samples

The previously-prepared aqueous suspension of GO was mixed with the TiO_2 crystalline suspension under stirring at room temperature for 1 h and under sonication for another 1 h. Different amounts of GO were used to prepare suspensions with GO concentrations ranging from 1 to 5 wt%. It was observed that suspensions with concentrations of GO above 5 wt% did not give rise to uniform coatings, which negatively affected the optical transparency of the obtained films.

Soda-lime glass slides (2.5 cm × 2.5 cm × 1 mm) were used as substrates in this work. These slides were initially washed with water and soap. Next, they were soaked in a Piranha solution (sulfuric acid (Synth / 98%) and hydrogen peroxide (Neon / 38 vol%) at a volume ratio of 3:1) at room temperature for 2 h. The slides were then carefully washed with deionized water and air-dried at room temperature. They were subsequently sonicated in EtOH and dried in air again. The coating step was conducted by dip-coating at a withdrawal speed of 2.7 mm/s. The glass slides were dipped into the previously-prepared TiO_2 and TiO_2-GO suspensions. The number of layers deposited on the

substrates was 1, 5, or 10 layers. A drying step was performed in air at 70 °C for 10 min after the deposition of each layer. It was observed that such coatings showed a satisfactory adherence to the glass substrate as they could be handled and cleaned with soft paper and alcohol without peeling. Powdered materials were also obtained to evaluate the bandgap energy (E_g) of the prepared materials by UV–Vis diffuse reflectance spectroscopy (UV–Vis DRS). These specimens were prepared after drying the TiO_2 and TiO_2-GO solutions in air at 70 °C overnight.

Coated samples were calcined in air at 400 °C for 2 h with a heating rate of 5 °C/min to evaluate the influence of this step on their properties. It was also investigated the effect of UV radiation on the reduction of GO to RGO. For this purpose, as-prepared samples were illuminated to UV light for 3 h using an 18 W UVA lamp (Osram Dulux S Blue / maximum emission at 354 nm) and kept at 5 cm away from the samples. The irradiation chamber was air-ventilated to keep samples at room temperature during this step. As will be addressed further on, this irradiation step promoted the reduction of Go to RGO and gave rise to the TiO_2/RGO composites studied in this work. As-prepared samples were designated as TiO_2-GO/X, where X represents the concentration of GO in wt.%. Coatings exposed to UV radiation were labeled as TiO_2-GO/X/UV, while those heat-treated were identified as TiO_2–GO/X/HT. Fig. 1 displays a scheme of the experimental work performed in this study.

2.4. Characterization of the synthesized materials

A Philips-PANalytical PW 1710 diffractometer was employed to conduct XRD tests at a step size of 0.06°, within the 2-theta range of 20–70°, and using an acquisition time of 3 s. CuKα radiation (λ = 1.54 Å) was used in these tests. A WiTec Alpha 300 system with excitation radiation of 632.82 nm (He-Ne laser / 1 mW) was used to conduct Raman spectroscopy under ambient conditions. The spectra were taken from 154 to 2735 cm^{-1} and considering 6 acquisitions per min. A Shimadzu UV-2600 spectrometer was used to evaluate the optical transparency and E_g of the prepared materials. The optical transparency was assessed after the positioning of the glass slides in the spectrometer and the measurement of the transmitted beam intensity. E_g was determined using powdered samples dispersed in barium sulfate (Shimadzu). It was used a diffuse reflectance accessory at a resolution of 1 cm^{-1}. The Kubelka-Munk and Tauc methods were used in these calculations [36]. The morphology of the prepared coatings was evaluated by SEM and AFM. AFM was conducted on Asylum Research MFP-3D and Park Systems XE-70 microscopes operating in the tapping and non-contact modes, respectively. Silicon cantilevers with spring constants of 26 or 130 N/m and resonance frequencies of 30 or 330 kHz were employed in these tests. The collected images were examined in the XEI software® provided by Park Systems. SEM was performed on an FEI Quanta 200 field emission gun (FEG) microscope at an accelerating voltage of 15 kV. The electrical conductivity measurements by a DC four-probe method were performed using a Jandel Universal Probe (Engineering ltd. Leighton Buzzard) coupled with a Keithley 238 high current measuring unit. In these tests, four probes were arranged in a line and at a distance of 1.0 mm from each other. To determine the electrical resistance values, films with different thicknesses were prepared. The data were collected at 3 different points on each film. The calculations of the electrical conductivity values were obtained using the mathematical treatment described elsewhere [37]. The thickness of each film was measured in 5 different regions with a Mitutoyo Absolute system. Such thicknesses were also measured by SEM microscopy, using the aforementioned electron microscope. The thickness values used in the calculations to determine the conductivity were the average value obtained. The current flowing through the examined specimens was monitored as a function of the applied voltage.

2.5. Wettability tests

The wetting behavior of the prepared films was evaluated by measuring the water contact angle (WCA). WCA was evaluated at room temperature using a Dino-Lite AM2111 digital microscope. A photograph was taken about 10 s after dripping water on the substrate. WCA was measured taking into account at least three sessile droplets with 3 μL. This property was initially evaluated over time for assessing the effect of the aging step on the wettability behavior of the fabricated materials. For this purpose, samples were kept in dark conditions to avoid the influence of natural UV radiation on these experiments. Next, WCA was measured after illuminating samples with UVA light for investigating the so-called photoinduced superhydrophilicity. Such tests were conducted using the aforementioned UV chamber. The electrically

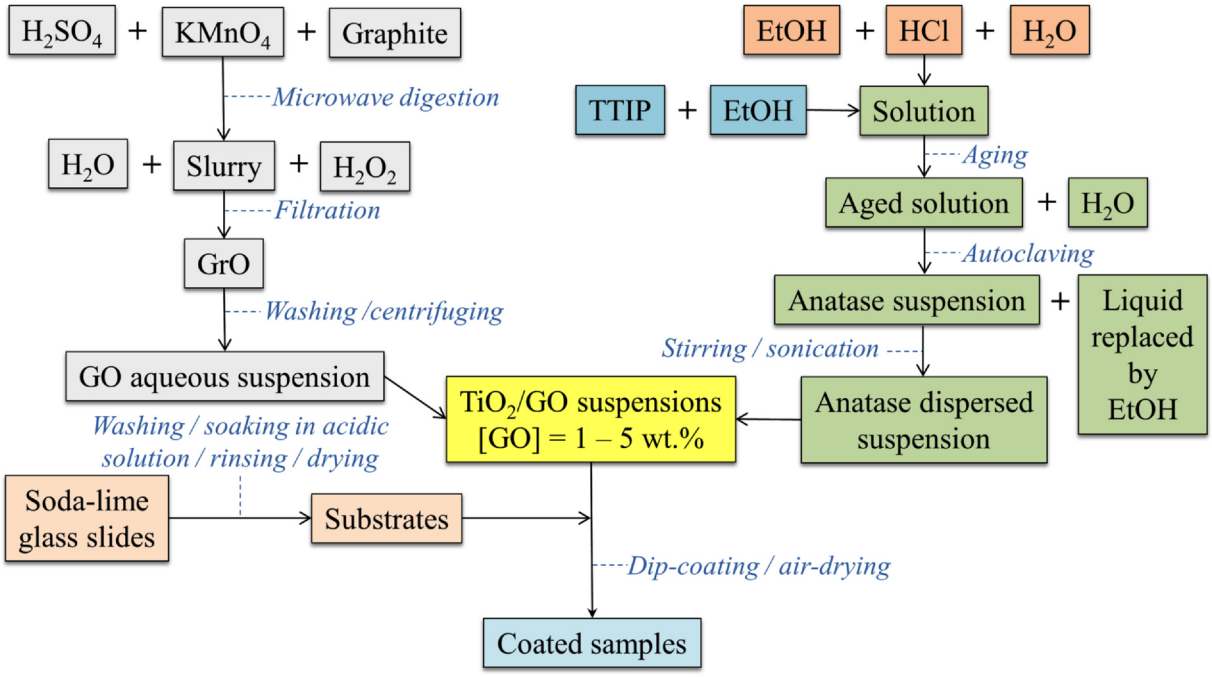

Fig. 1. Scheme of the experimental work performed in this study.

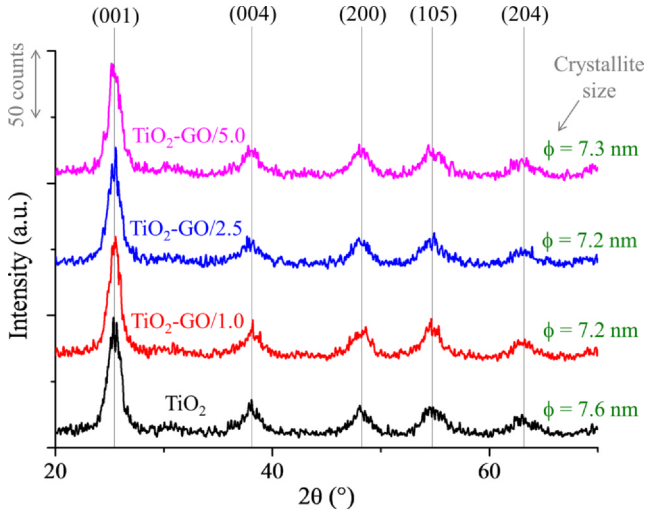

Fig. 2. XRD patterns of powdered samples in the as-prepared condition. The highlighted diffraction peaks are related to anatase. The crystallite size evaluated by the Scherrer equation is also exhibited.

induced superhydrophilicity was measured by applying a DC voltage on indium tin oxide (ITO) substrates coated with TiO_2-GO composites. WCA was evaluated as described before.

3. Results and discussion

Fig. 2 shows the XRD patterns collected in this work for powdered samples in the as-prepared condition, as well as the crystallite size estimated after applying the Scherrer equation to the crystal plane (0 0 1). It can be noted that TiO_2 shows a crystallite size below 8 nm. The diffraction lines highlighted in this Figure are all associated with anatase (JCPDS file number 21-1272). This result reveals that the hydrothermal treatment was effectively crystallized TiO_2 into anatase nanoparticles, which is in line with previous studies [30,31]. Fig. 3 displays the Raman spectra of as-prepared and UVA-illuminated composite coatings. The spectrum of a TiO_2 coating is also displayed for reference purposes. E_g, B_{1g}, B_{1g} + A_{1g}, and E_g vibration modes of anatase are observed at 145, 405, 520, and 640 cm^{-1}, respectively [38]. The D and G bands of graphene are noted at about 1330 and 1600 cm^{-1}. Such bands have been ascribed to defects in the graphene network and in-plane vibration of sp^2-bonded carbon atoms [39,40]. The observation of Raman bands ascribed to graphene reveals that it was successfully incorporated into the TiO_2-based films. It can also be noted that the larger the concentration of GO in the composite, the more intense are the graphene-related absorption bands and the less intense are the features due to titania. Furthermore, the D and G bands of graphene are no longer observed after the heat treatment in air, revealing that GO could be burned during this step. Table 1 gives the intensity ratio between the D and G bands for the composites prepared in this study. It can be noted that this ratio is larger the higher the GO loading, which reveals a greater disorder in the composite structure [41]. Moreover, I_D/I_G tended to increase after the UV-irradiation of the coatings, indicating an increase in the concentration of defects or edge areas from GO to RGO [42]. This behavior was not observed for TiO_2-GO/5.0, which experienced a decrease of the I_D/I_G ratio from 1.84 to 1.56 when it was exposed to UVA light for 3 h. This may be due to a fast photocatalytic reduction of GO by TiO_2 during the composite illumination with UVA light, which was also reported by Akhavan *et al.* [43].

Fig. 4 displays the transmittance spectra of samples coated with either TiO_2 or TiO_2-GO. The spectrum collected for a bare glass substrate is also shown for comparison purposes. One notices that all samples exhibited a significant decrease in the amount of light transmitted in the UV region, which is related to the jump of electrons across the forbidden band. Indeed, as it will be demonstrated further on, the films prepared here have E_g varying from 3.20 to 3.12 eV, which corresponds to photons with wavelengths from about 387 to 397 nm. This means that photons with these wavelengths can be absorbed by valence-band electrons, which promotes them to the conduction band. The bare glass substrate showed a similar behavior because it also has E_g within the UV region [44]. It is worth highlighting the high optical transparency of the films prepared in this work within the visible region (around 70% at 600 nm). This behavior is mandatory for the use of coatings in many applications, for instance, in the fabrication of self-cleaning windows [24]. The digital photography provided in Fig. 4 reinforces the optical transparency of these films, in which it is possible to read what is written below the glass slides. The glass slides intentionally show coated and uncoated regions due to a partial dip of the substrates into the prepared suspensions. It was observed that the higher the concentration of GO, the lower was the optical transparency within the visible region. We noticed that the increase of the GO loading gave rise to dark coatings, which justifies the smaller transmittance displayed by composites containing high concentrations of this material. As aforementioned, films prepared with GO loadings above 5 wt% were inhomogeneous and showed low optical transparency.

Fig. 5a exhibits AFM images taken for the coatings obtained in this work. An image obtained for a bare glass substrate is also displayed. The glass slide has a smooth surface, which is why it was chosen as the substrate in this work. The way GO sheets are deposited on a substrate can greatly influence the thickness and roughness of the coatings obtained. During the dip-coating process, viscous forces drag the solution upwards due to the withdrawal of the substrate from the solution, leading to the formation of a meniscus. Such a viscous drag is proportional to both the liquid viscosity and withdrawal speed of the substrate [45]. A high withdrawal speed can cause the GO sheets to lose orientation, giving rise to an irregular surface with a high concentration defects and causing an increase in film thickness and roughness [46]. As the withdrawal speed used in this study was kept as low as 2.7 mm/s, the difference in the AFM images exhibited in Fig. 1 may be related to the different viscosities of the TiO_2-GO suspensions prepared. Moreover, the solvent (EtOH) evaporation could also affect the organization of GO sheets in the obtained films.

Fig. 5b shows the roughness of these coatings as a function of the GO concentration. Two different parameters of surface roughness are displayed in this Figure, namely Ra and RMS. Ra is the average roughness of a surface, evaluated taking into account peaks and valleys. RMS, on the other hand, is the root mean square of this roughness. Ra and RMS are based on the same height measurements of surface peaks and valleys, but the calculation procedure is different [47]. The bare glass substrate showed Ra and RMS of 0.25 and 0.32 nm, which reinforces the smoothness of this surface. It can be observed that Ra and RMS became larger when the GO loading was increased. This behavior can be associated with the stacking of GO sheets as its concentration is increased. Moreover, GO sheets have micrometers-long wrinkles and oxygenated groups at their edges where the agglomeration of TiO_2 nanoparticles may take place [48], which can also increase the surface roughness [49]. However, it is worth highlighting that the films prepared in this work exhibited a roughness of a few nanometers. According to Busscher *et al.* [50], the wettability of surfaces with Ra below 100 nm is not affected by their roughness. Thus, this property was not taken into account when investigating the wettability behavior of materials containing different concentrations of GO.

The bandgap energy (E_g) for a semiconductor can be evaluated by plotting $[F(R)h\nu]^n$ as a function of $h\nu$, where F(R) represents the so-called extinction coefficient, h the Planck constant (4.14×10^{-15} eV.s), and ν the photon frequency (Hz). F(R) can be calculated from Equation (1), where R (%) is the reflectance measured by UV–Vis DRS:

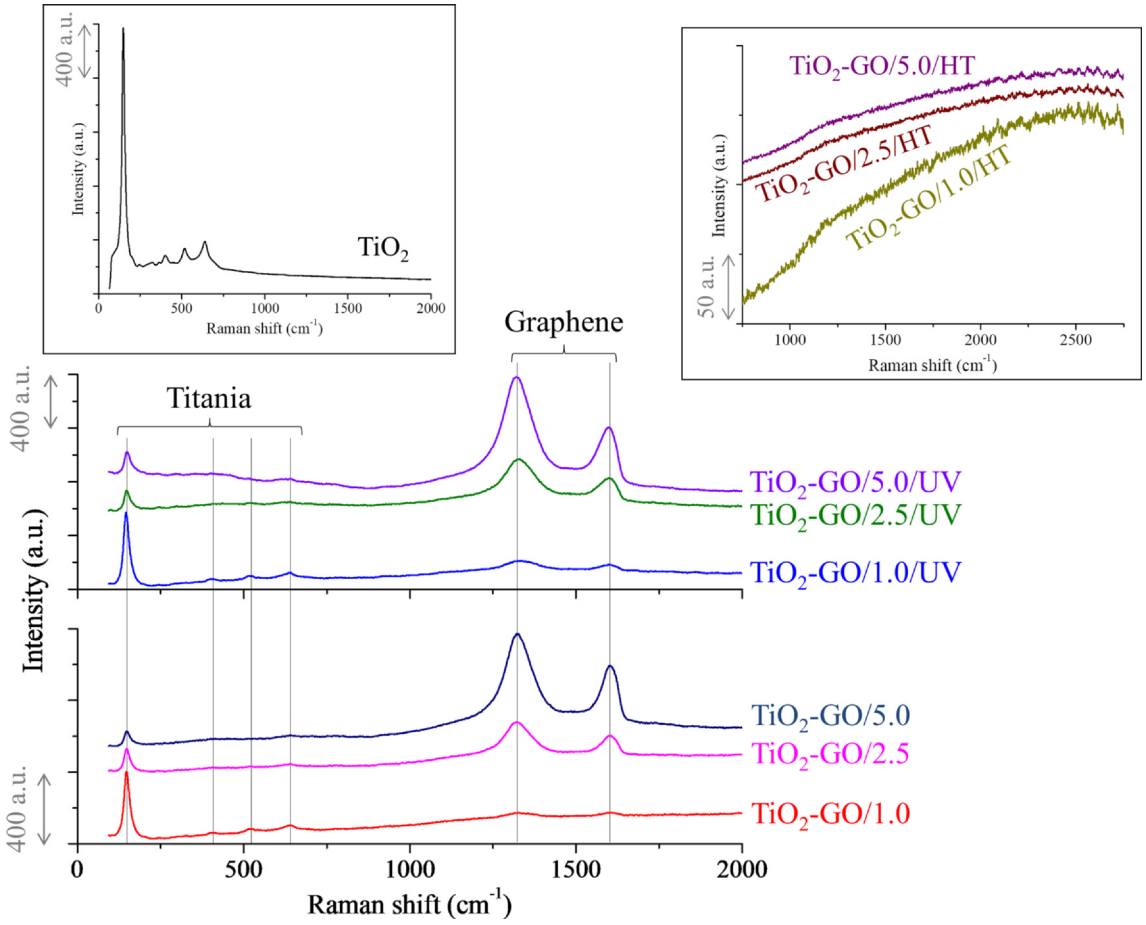

Fig. 3. Raman spectra of samples coated after 5 dipping cycles. The spectrum of a TiO_2 coating is also exhibited for reference purposes.

Table 1
Intensity ratio between the D and G bands (I_D/I_G) observed in the Raman spectra of composite coatings prepared in this work.

Sample	I_D/I_G
TiO_2-GO/1.0	1.45
TiO_2-GO /1.0/UV	1.71
TiO_2-GO /2.5	1.80
TiO_2-GO /2.5/UV	1.85
TiO_2-GO/5.0	1.84
TiO_2-GO/5.0/UV	1.56

$$F(R) = \frac{(1-R)^2}{2R} \quad (1)$$

The index n is related to the transition experienced by an electron when it is promoted from the valence band to the conduction band. It has been reported that n = ½ for an indirect allowed transition, n = 2 for a direct allowed transition, n = 3 for an indirect forbidden transition, and n = ⅔ for a direct forbidden transition [51]. Direct allowed transitions occur when the electron is directly promoted to the conduction band with no absorption or emission of phonons. Direct forbidden transitions require the participation of phonons to conserve system momentum and are less likely to occur. Indirect transitions are observed when at least one phonon participates in the absorption or emission of another phonon to conserve momentum. Both direct and indirect transitions can take place in semiconductors [52]. TiO_2 has a direct forbidden gap, which is also degenerated in an indirect allowed transition. As a consequence, we considered n = ½ in our calculations as recommended elsewhere [36]. E_g is given by intercepting with the x-axis the line tangent to the inflection point of $[F(R)h\nu]^{1/2}$ versus $h\nu$.

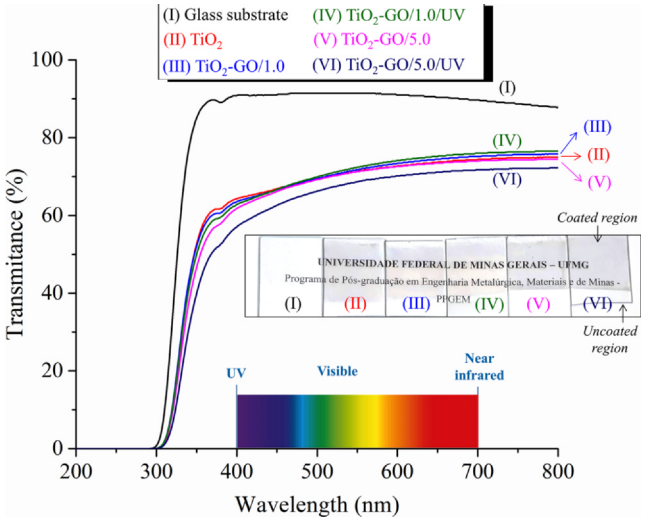

Fig. 4. Transmittance spectra of glass substrates coated with either TiO_2 or TiO_2-GO films. The spectrum taken for a bare substrate is also exhibited for comparison purposes. The coated samples were obtained after 1 dipping cycle. Inset: digital photograph of the samples prepared in this study.

Fig. 6a and 6b exhibit, respectively, the plot of $[F(R)h\nu]^{1/2}$ versus $h\nu$ and E_g as a function of the graphene concentration. TiO_2 showed E_g around 3.20 eV, which is the value commonly reported for anatase [53,54]. E_g became smaller when the concentration of GO was increased. The illumination of the coated samples with UVA light for 3 h

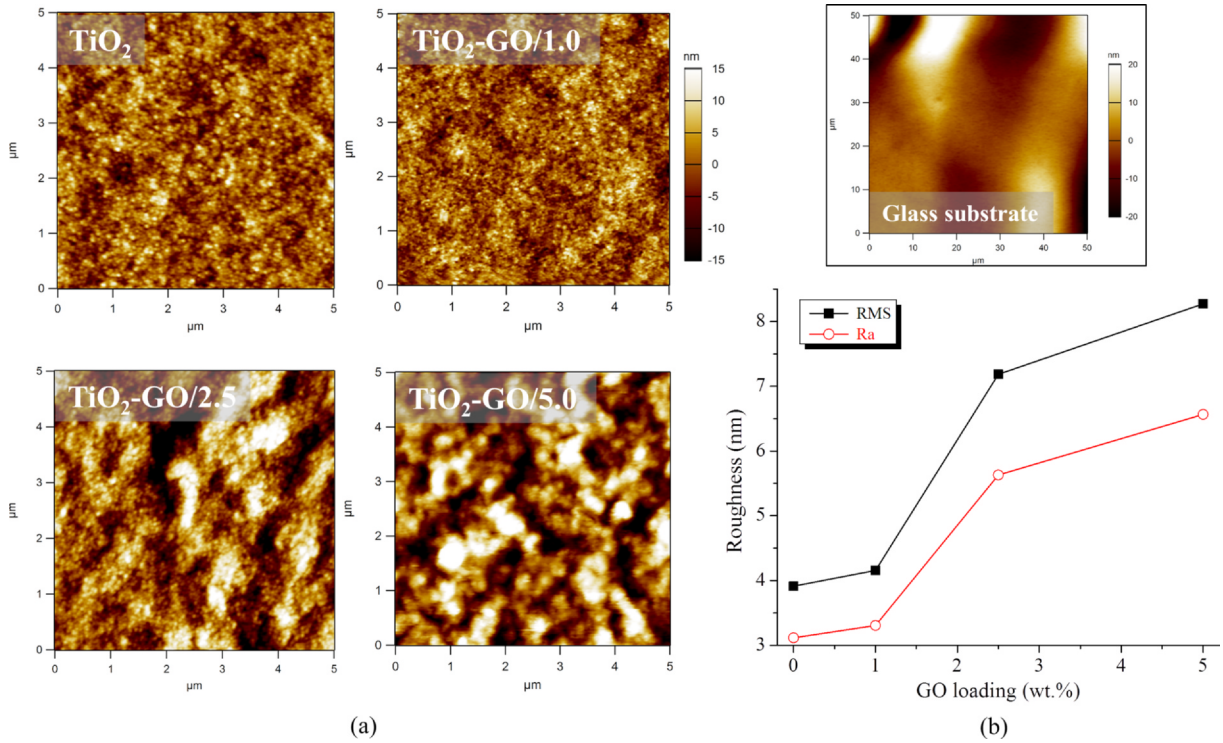

Fig. 5. (a) AFM images and (b) roughness measured for the coatings obtained in this work. Coatings obtained after 1 dipping cycle. Inset: AFM image collected for a bare glass substrate.

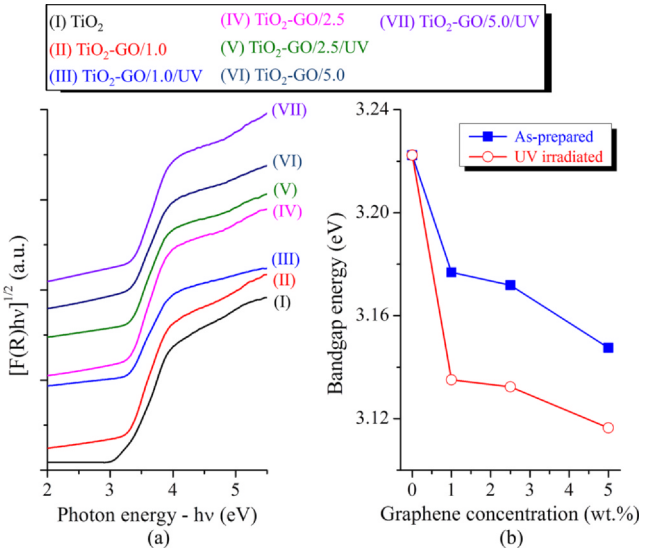

Fig. 6. (a) $[F(R)h\nu]^{1/2}$ as a function of the photon energy and (b) E_g as a function of the graphene concentration in the prepared nanocomposites.

led to a further decrease in E_g. This behavior can be related to the reduction of GO to RGO during the UV irradiation [42,55,56], which gave rise to TiO_2-RGO composites with narrower bandgaps than TiO_2 and TiO_2-GO. It is well established that highly-reduced GO is a good conductor and shows no gap [57]. Due to these properties, the reduction of GO to RGO is essential for the preparation of self-cleaning TiO_2-based coatings. The decrease of E_g with the increase of GO concentration is related to the narrow bandgap displayed by this material in its reduced state, which tends to decrease the composite bandgap. As highly-reduced GO has no bandgap, it is plausible to expect E_g to decrease as the GO loading in the prepared samples increases. Moreover, the decrease in the composite bandgap energy when GO was reduced to RGO may reveal the formation of Ti-O-C interfacial bonds [58]. These chemical bonds can give rise to a pathway for charge transfer, which slows down the recombination of electron-hole pairs generated during UVA illumination [59]. The presence of RGO in UV-irradiated samples has motivated the electrical characterization of these materials and an investigation of how their wettability can be controlled by applying a DC voltage on them.

Fig. 7a exhibits the electrical current flowing through the samples as a function of the applied voltage. All samples displayed a linear increase of current (i) with voltage (V), revealing that they follow Ohm's law in the examined voltage range. One can infer the resistivity (ρ – Ω.m) of the tested materials from the curves shown in Fig. 7a and Equation (2), where w is the coating thickness (m) and F is a dimensionless correction factor related to the shape, length/width ratio, and arrangement of the samples used in the electrical tests. In this work, F was evaluated following a procedure described elsewhere [37], which gave rise to a value of 4.45.

$$\rho = \frac{V}{i} wF \tag{2}$$

Fig. 7b depicts the thickness, resistivity, and sheet resistance (R_S – Ω/Sq) of the obtained films. R_S is given by the ratio between ρ and w. We observed that the film becomes thicker when the number of layers deposited on the glass slide is increased. For instance, TiO_2 and TiO_2-GO/1.0/UV samples obtained after 5 dipping cycles were 0.48 ± 0.05 µm and 0.19 ± 0.06 µm thick, whereas coatings prepared after 10 cycles were 1.86 ± 0.25 µm and 1.11 ± 0.25 µm thick, respectively. This finding can also be noticed in the cross-sectional SEM micrographs displayed in Fig. 7b. This increase in thickness was accompanied by a decrease in R_S. In particular, the increase in the number of dipping cycles from 5 to 10 decreased R_S from 7.4×10^8 to 2.0×10^8 Ω/Sq for TiO_2, and from 3.8×10^8 to 5.3×10^7 Ω/Sq for TiO_2-GO/1.0/UV. As R_s is inversely proportional to the film thickness, it is reasonable to expect that thicker films have lower R_S. It can also be noticed that the addition of GO decreased the electrical resistivity of TiO_2. For instance, the value of ρ evaluated for TiO_2 and TiO_2-GO/5.0/

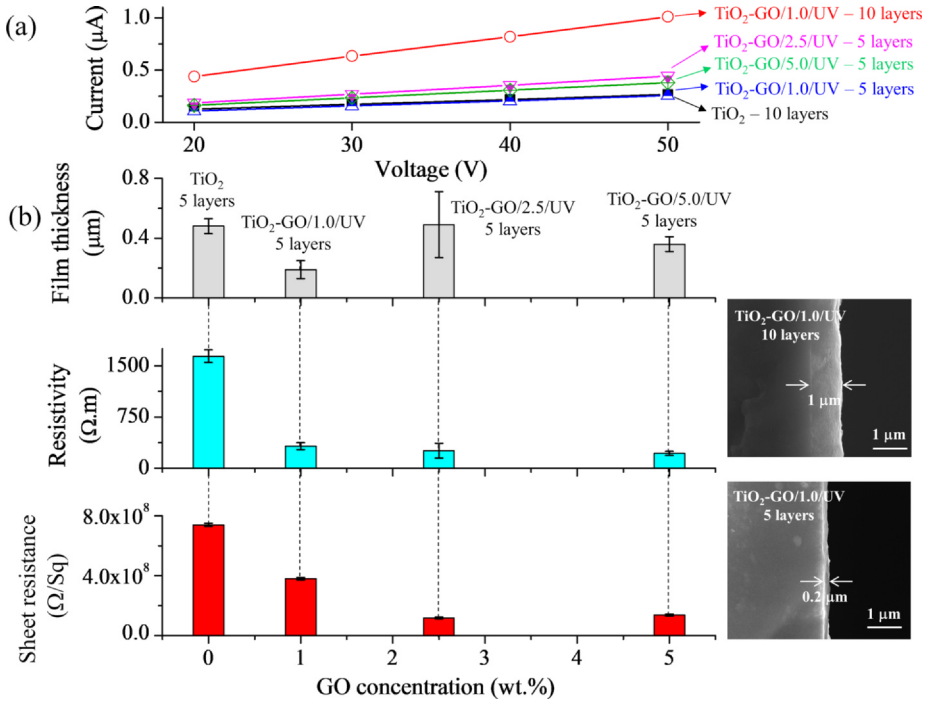

Fig. 7. (a) Electrical current flowing through samples as a function of the applied voltage. (b) Thickness, resistivity, and sheet resistance of films prepared in this study. Cross-sectional SEM micrographs of coated samples are also shown.

UV were, respectively, 1639 and 220 Ω.m, which represents a decrease of over 7 times. As discussed before, the UV irradiation of GO-containing samples causes the reduction of GO to RGO. As RGO is a good conductor, it is plausible to expect that the higher its concentration in the prepared coatings, the better their electric conduction should be. The RGO-containing films prepared herein show good electric conducting properties, which could be interesting in many applications such as in the preparation of coatings with antistatic properties to inhibit the adhesion of pollutants on coated surfaces [24].

Table 2 brings the values of R_s reported in this work and the literature for graphene-based coatings. Becerril *et al.* [60] investigated the electrical and optical properties of GO and RGO thin films prepared by spin coating. As already expected, they observed that the reduction of GO to RGO greatly decreased R_S. The treatment with hydrazine vapor followed by a heat treatment under argon flow at 400 °C was effective to promote the reduction of GO to RGO, leading to films with R_S of about 10^5 Ω/Sq. Yin *et al.* [61] prepared RGO films by the chemical reduction of GO on polyethylene terephthalate substrates. The materials prepared by them displayed R_S around 10^3 Ω/Sq, which, according to the authors, could allow their use in the preparation of flexible organic photovoltaic devices. Wang *et al.* [62] obtained highly-conducting (R_S around 10^3 Ω/Sq) and optically transparent RGO films by transfer printing on quartz substrates, followed by annealing and graphitization at 400 and 1100 °C. The authors report that the properties displayed by the prepared materials could allow their application in transparent conductors for touch panels. Huang *et al.* [63] fabricated RGO/single-wall carbon nanotubes (SWCNTs) composite films. As both materials are good conductors, the prepared films displayed R_S as low as 10^2 Ω/Sq. Similar values of R_S were also reported by Park *et al.* [64] for thin SWCNTs films. Although these materials have a greater conduction capacity than the films prepared here, the coatings investigated in this study may also show photocatalytic properties due to the presence of TiO_2, which can be interesting in many applications including the photodegradation of pollutants and living microorganisms such as bacteria and fungi [65]. Akhavan *et al.* [43] obtained TiO_2-RGO coatings after anchoring TiO_2 nanoparticles on RGO sheets. Thin layers were deposited between gold electrodes to evaluate the electrical conductivity of the prepared materials. The fabricated coatings showed R_S around 10^6 Ω/Sq, a value below those obtained in this work. Nonetheless, the experimental work followed by the authors is more complex than that suggested here since multi-steps are needed, which can be time-consuming and expensive.

Table 2
Sheet resistance reported in this work and the literature for graphene-based coatings.

Sample	Sheet resistance (Ω/Sq)	Reference
TiO_2	7.4×10^8	This work
TiO_2-GO/1.0/UV	3.8×10^8	This work
TiO_2-GO/2.5/UV	1.2×10^8	This work
TiO_2-GO/5.0/UV	1.4×10^8	This work
GO	1.0×10^{12}	[60]
RGO (Hydrazine)	1.0×10^8	[60]
RGO (Hydrazine + annealing at 400 °C under argon flow)	1.0×10^5	[60]
RGO (Thermal reduction at 1000 °C under argon / hydrogen flow (1:1))	3.2×10^3	[61]
RGO (Hydrazine and ammonium hydroxide solutions + annealing at 400 and 1100 °C under vacuum and argon flow)	2.0×10^3	[62]
RGO-SWCNT (Hydrazine)	2.5×10^2	[63]
Carbon nanotube (Annealing at 400 °C + acid treatment)	3.0×10^2	[64]
TiO_2-RGO (Photocatalytic reduction with UV light)	4.6×10^6	[43]

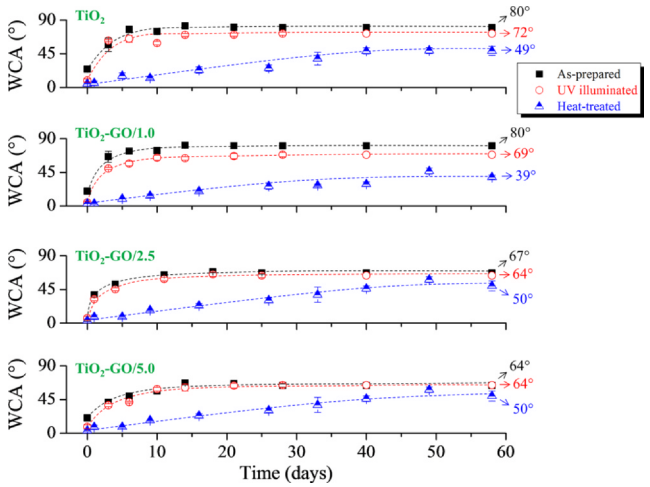

Fig. 8. WCA as a function of the aging time for as-prepared, UV-irradiated, and heat-treated samples. Samples obtained after 1 dipping cycle. The dashed lines connecting the data points are used as a guide to the eyes only.

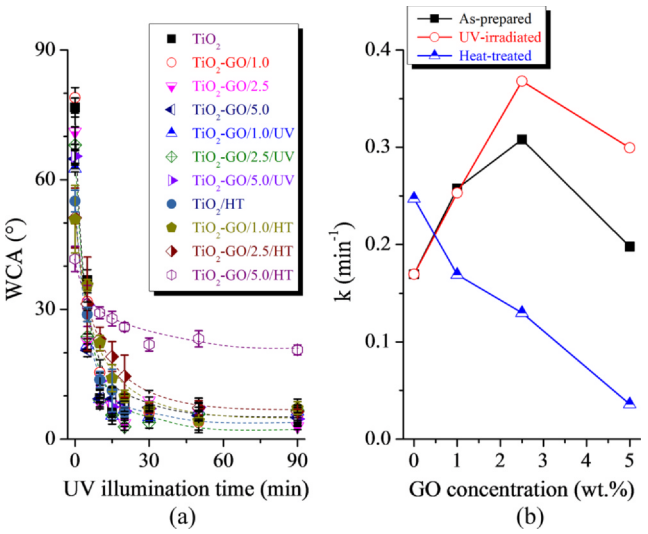

Fig. 9. (a) WCA as a function of the irradiation time with UVA light of samples previously aged in air for about 60 days. (b) Values of k assessed for the tested materials. The lines connecting the data points are used as a guide to the eyes only. Samples obtained after 1 dipping cycle.

Fig. 8 exhibits WCA as a function of the aging time for as-prepared, UV-irradiated, and heat-treated samples. One observes that WCA rapidly increased over time, reaching a plateau after about 15 days for as-prepared and UV-irradiated specimens [32]. The heat treatment step had a great effect on WCA, leading to smaller contact angles. The heat treatment promotes the removal of residual alkoxy groups derived from the sol-gel synthesis of TiO_2. It is worth remembering that the as-prepared samples were only air-dried at 70 °C for 10 min. As carbon-containing compounds are hydrophobic, the removal of organic residues increases the wettability of the heat-treated coatings. Besides, it has been reported that the heat-treatment of sol-gel TiO_2 increases both the strength of Ti-O-Ti bonds and the surface energy of titania with the atmosphere [14]. The wetting angle (θ) of a surface is given by a balance of the interfacial energies at the solid-vapor (γ_{sv}), solid-liquid (γ_{sl}), and liquid-vapor (γ_{lv}) interfaces. This relation is expressed by Young's equation. From Equation (3), it is clear that the higher γ_{sv}, the smaller θ should be.

$$\cos\theta = \frac{\gamma_{sv} - \gamma_{sl}}{\gamma_{lv}} \tag{3}$$

From Fig. 8, one notes that both TiO_2 and TiO_2-GO/1.0 reached similar values of WCA in the as-prepared condition, around 80° after about 60 days of aging. Further additions of GO led to smaller WCAs; the values observed for as-prepared TiO_2-GO/2.5 and TiO_2-GO/5.0 were 67 and 64°, respectively. In a general way, the irradiation of the coatings with UVA light decreased the WCA measured after 60 days. This behavior was most dramatic for TiO_2, TiO_2-GO/1.0, and TiO_2-GO/2.5. It can be related to the creation of electron-hole pairs upon UV illumination, which could change the surface energy of the composite materials [9,24,66]. Moreover, UV irradiation also promotes the removal of organic pollutants adsorbed on the coating surface due to the occurrence of photocatalytic reactions [24].

The photoinduced superhydrophilicity of samples previously aged in air for about 60 days was evaluated after their illumination with UVA light. Fig. 9a displays WCA as a function of the irradiation time. All samples exhibited a sharp decrease in WCA when they were exposed to UVA light. Several samples showed WCAs below 10° after 90 min of irradiation, which is within the angle range typically reported for superhydrophilic materials [67]. The so-called Israelachvili-Gee model [68] describes the wetting behavior of biphasic heterogeneous surfaces. It is associated with Equations (4) and (5), where θ is the contact angle measured for a liquid dripped on a heterogeneous surface, f_1 and f_2 are the volume fractions of phases 1 and 2, θ_1 and θ_2 are the contact angles measured on homogeneous surfaces of these phases.

$$f_1 + f_2 = 1 \tag{4}$$

$$(1 + \cos\theta)^2 = f_1(1 + \cos\theta_1)^2 + f_2(1 + \cos\theta_2)^2 \tag{5}$$

If we consider that θ_1 represents the contact angle measured on an uncontaminated TiO_2 surface, θ_2 the angle evaluated on a surface contaminated with organic pollutants after keeping it exposed to air, and both θ_1 and θ_2 are known, it is possible to calculate f_2 from Equations (4) and (5). In this work, we considered $\theta_1 = 4°$ and $\theta_2 = 90°$ as suggested elsewhere [69].

The photoinduced superhydrophilicity can be described by a Langmuir-Hinshelwood-based kinetic model expressed in Equation (6), where k (min^{-1}) is a pseudo-first-order rate constant, $(f_2)_{t=0}$ is the surface fraction covered by organic pollutants at the initial time, and $(f_2)_t$ is the surface coverage after illumination with UV light for a time t.

$$\ln(f_2)_t = \ln(f_2)_{t=0} - kt \tag{6}$$

Thus, k can be evaluated by plotting $\ln(f_2)$ as a function of t, in which this rate constant is given by the slope of the obtained straight line. Fig. 9b shows the values of k calculated for the tested samples. The addition of GO caused an increase in k for as-prepared and UV-irradiated samples. Nonetheless, UV-illuminated materials showed larger values of k than the as-prepared ones when 2.5 and 5.0 wt% GO loadings are taken into account. The increase of the GO concentration from 2.5 to 5.0 wt% decreased k for as-prepared and UV-irradiated samples, which can be related to the stacking of GO sheets. The stacking of these sheets may prevent UV light from reaching TiO_2 particles, negatively impacting both the generation of electrons and holes by UV light and the photoinduced superhydrophilicity of the composite [1,70]. Besides, TiO_2/GO/5.0 and TiO_2/GO/5.0/UV may show a highly-negative surface, which may decrease the separation of the electron-hole pairs and lead to fast recombination of these charge carriers [28].

As discussed before, the UV irradiation of GO causes its reduction to RGO [42,55,56]. RGO can act as an accessible migration pathway for electrons and holes photogenerated in TiO_2, which extends the life of these charge carriers. In the absence of RGO, the recombination of electrons and holes in TiO_2 is more likely, which adversely affects its superhydrophilicity. As a consequence, RGO plays a key role in the photoinduced superhydrophilicity of TiO_2-RGO composites. The difference in the rate constant k measured for TiO_2/GO/2.5, TiO_2/GO/5.0, TiO_2/GO/2.5/UV, and TiO_2/GO/5.0/UV is ascribed to the previous

formation of RGO in UV-irradiated samples. Nonetheless, this difference is not evident for TiO_2/GO/1.0 and TiO_2/GO/1.0/UV because perhaps the GO concentration in these materials is too small. Anadan *et al.* [24] also reported that the value of k for composite TiO_2-RGO films was higher than that evaluated for pure TiO_2 films. It was observed that WCA reached values of about 5° after 180 min of exposure of TiO_2-RGO films to UV light. Similarly, Zhu *et al.* [25] reported that TiO_2-RGO hetero-structured films showed electrical conductivity, transparent properties, and photoinduced superhydrophilicity, showing WCA around 4.2° after UV illumination. Sakai *et al.* [56] observed a higher hydrophilic conversion rate for TiO_2-RGO films when compared to TiO_2 coatings. Moreover, a reversible hydrophilic/hydrophobic conversion was observed in at least 7 cycles, without dramatic changes in the obtained absorption spectra. Prabhu *et al.* [26] showed that the photoinduced superhydrophilicity of TiO_2-RGO composites tends to be more pronounced when the concentration of RGO is increased.

After 60 aging days, the heat-treated samples reached WCAs between 40 and 50°, corresponding to high hydrophilicity. The kinetic constant k ascribed to the photoinduced superhydrophilicity of these materials decreased when the GO concentration was increased (Fig. 9b). This behavior can be associated with partial combustion of GO when these samples were calcined in air at 400 °C for 2 h [71]. One could expect that the higher the loading of GO, the smaller the concentration of TiO_2 in the composite. As a consequence, the burning of GO led to poorer coatings in TiO_2, which may justify the decrease of k when the GO concentration was increased. Indeed, Raman tests revealed that GO burning occurred when the composites were heat-treated in air (Fig. 3). The larger k displayed by the heat-treated TiO_2 when compared to either as-prepared or UV-irradiated TiO_2 samples can be ascribed to the aforementioned removal of residual alkoxy groups from it during the heat treatment.

Aiming to investigate how the wettability of the composites prepared in this study is influenced by the flow of an electrical current, a DC potential difference was applied to these materials. This procedure was conducted as schematically exhibited in Fig. 10a. The coatings were initially deposited on an indium tin oxide (ITO) substrate, which is a good electrical conductor and an optically transparent material [72]. The dipping step was performed as previously described and 5 layers were deposited on each ITO substrate. A voltage was then applied on the substrate, while WCA was monitored over time. The electrical current flowing through the examined samples was initially kept constant at 0.2 A, whereas the voltage needed to reach this current value varied from one sample to another. From Fig. 10b, it can be observed that the bare ITO substrate showed a WCA nearly constant at about 80° up to 45 s when it suddenly decreased to 0°. This behavior is ascribed to the evaporation of the water droplet. It can be shown from Joule's and Ohm's laws that a current of 0.2 A at a potential of 10 V for 40 s gives an electric power of 80 J, which is high enough to evaporate a 3 μL water droplet. The composite films displayed a different behavior, where a continuous decrease of WCA was observed over time. The final reduction of WCA to 0° is also due to the evaporation of water, but this phenomenon is preceded by the spreading of the water droplet on the coating surface. Moreover, it can be noticed that the time required for the complete removal of water is shorter for the composite films than for the ITO substrate. TiO_2-GO/2.5/UV took less time than TiO_2-GO/1.0/UV to the complete spreading of water, which can be related to the smaller resistivity of the former (Fig. 7).

To avoid the evaporation of the water droplet due to the Joule's effect, further tests were performed keeping the current fixed at 0.01 A, a value theoretically insufficient to evaporate a 3 μL droplet. The composite films exhibited similar behavior, in which there was a continuous decrease in WCA over time until the water droplet was completely spread on the ITO surface. On the other hand, WCA remained nearly constant over time for the bare ITO substrate since there was no evaporation or spreading of water. Electrons and holes that flow through the composite film by the action of the applied voltage play an important role in the spreading of water on it. Fig. 10c shows photographs of the spreading of a water droplet on an ITO substrate as a function of time when a DC voltage is applied on the latter.

The electrically-induced hydrophilicity of the samples prepared in this study can be of great importance in several applications. It has been reported that changes in surface wetting have a significant effect on surface properties and can influence interfacial interactions with liquids and gases. Moreover, these surface changes alter interactions with biomolecules such as DNA, RNA, and proteins, and change the response of cells and tissues that come into contact with the surface [73]. The

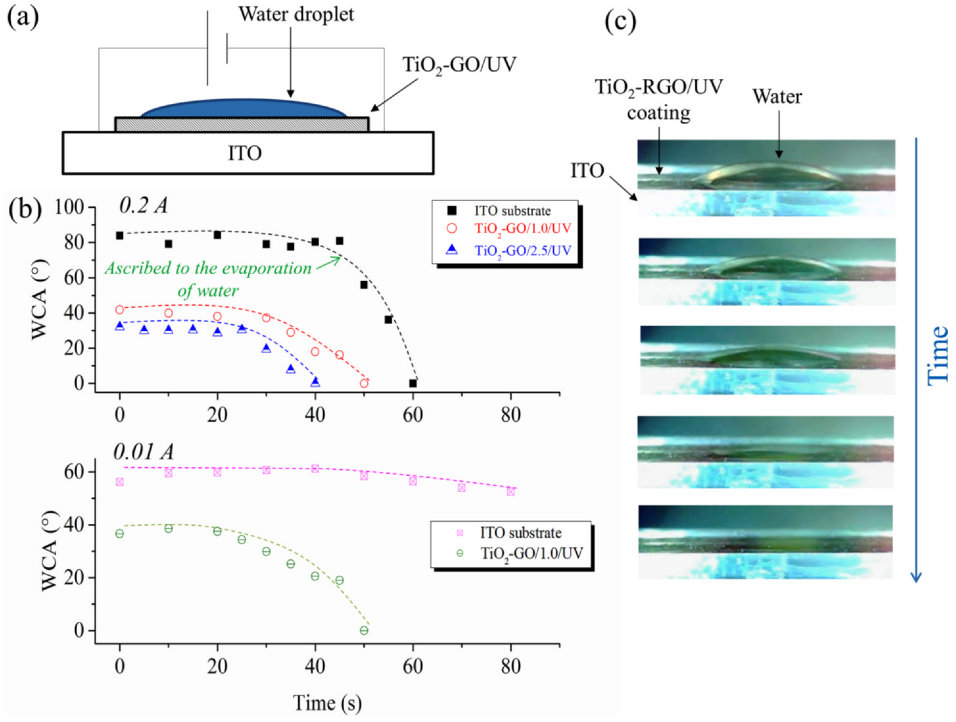

Fig. 10. (a) Schematic of the setup used for evaluating the electrically-induced superhydrophilicity in TiO_2-GO composite films. (b) WCA as a function of time during the application of a DC potential difference on the ITO substrate. (c) Photographs taken at different times from an ITO coated sample during the application of a DC voltage. ITO was coated with TiO_2-GO/2.5/UV.

hydrophilic behavior triggered by the application of a small potential difference represents an essential feature of the specimens prepared herein, which makes them promising candidates for the preparation of smart materials [74]. This property will be further explored in the next work.

4. Conclusions

In this work, TiO_2 and TiO_2-RGO films were successfully prepared. It was investigated the structural, electrical, and wetting properties of these materials. The prepared samples displayed high optical transparency in the visible region of the electromagnetic spectrum, typically above 60%. The irradiation of GO-containing samples with UVA light caused the reduction of GO to RGO. This reduction was accompanied by a decrease in the E_g and electrical resistivity of the composite films. The increase in the GO concentration led to films with higher roughness and lower electrical resistivity. The UV irradiation and air-calcination of as-prepared films increased their hydrophilicity, which is related to the removal of residual organic groups. WCA increased over time when these samples were kept in air for about 60 days due to air pollution. The calcined samples showed the smallest values of WCA after this time, followed by UV-irradiated and as-prepared materials. The photoinduced superhydrophilicity of these samples was evaluated after irradiation with UVA light. WCA reduction kinetics was faster for UV-irradiated samples, especially for those containing either 2.5 or 5.0 wt% GO. However, the sample with a GO loading of 2.5 wt% and previously illuminated with UVA light was the one with the fastest kinetics. We also demonstrated that a superhydrophilic behavior could also be induced by applying a small DC voltage to the samples prepared here, which opens up new possibilities for the development of smart surfaces for several applications.

CRediT authorship contribution statement

Lucas M.C. Silva: Conceptualization, Methodology, Validation, Formal analysis, Investigation, Data curation, Project administration, Writing - original draft. **Bruno S. Gonçalves:** Investigation, Data curation, Writing - original draft. **Jorgimara de O. Braga:** Investigation, Data curation, Writing - original draft. **Tarcizo C.C. de Souza:** Methodology, Validation, Formal analysis. **Vinícius G. de Castro:** Data curation, Validation, Formal analysis. **Glaura G. Silva:** Resources, Methodology, Validation, Formal analysis. **Glenda R.B.S. Lacerda:** Data curation, Validation, Formal analysis. **Tulio Matencio:** Resources, Methodology, Validation, Formal analysis. **Tiago C. Barbosa:** Data curation, Validation, Formal analysis. **Carlos M. Viana:** Data curation, Validation, Formal analysis. **Manuel Houmard:** Conceptualization, Methodology, Validation, Formal analysis, Investigation, Data curation, Project administration, Resources, Writing - original draft, Funding acquisition, Supervision. **Eduardo H.M. Nunes:** Conceptualization, Methodology, Validation, Formal analysis, Investigation, Data curation, Project administration, Resources, Writing - original draft, Funding acquisition, Supervision.

Declaration of Competing Interest

The authors declare that they have no known competing financial interests or personal relationships that could have appeared to influence the work reported in this paper.

Acknowledgments

The authors thank the financial support from FAPEMIG (APQ-00792-17 / red-00102-16), CNPq (305013/2017-3 and 301423/2018-0), and CAPES (PROEX). UFMG Microscopy Center is acknowledged for the support provided in AFM and TEM. We also thank LEPCom and Prof. Rodrigo Oréfice for the great support given to this study. The authors express their gratitude to Prof. Herman Mansur, Alexandra Mansur, and Patrícia Azevedo from the Center of Nanoscience, Nanotechnology, and Innovation (CeNano^{2}I/CEMUCASI/UFMG) for the support provided in the AFM analyses.

References

[1] S.D. Perera, R.G. Mariano, K. Vu, N. Nour, O. Seitz, Y. Chabal, K.J. Balkus, Hydrothermal synthesis of graphene-TiO2 nanotube composites with enhanced photocatalytic activity, ACS Catal. 2 (2012) 949–956, https://doi.org/10.1021/cs200621c.

[2] H.-T. Ren, Q. Yang, Fabrication of Ag_2O/TiO_2 with enhanced photocatalytic performances for dye pollutants degradation by a pH-induced method, Appl. Surf. Sci. 396 (2017) 530–538, https://doi.org/10.1016/j.apsusc.2016.10.191.

[3] K. Siwińska-Stefańska, M. Fluder, W. Tylus, T. Jesionowski, Investigation of amino-grafted TiO_2/reduced graphene oxide hybrids as a novel photocatalyst used for decomposition of selected organic dyes, J. Environ. Manage. 212 (2018) 395–404, https://doi.org/10.1016/j.jenvman.2018.02.030.

[4] A. Miquelot, O. Debieu, V. Rouessac, C. Villeneuve, N. Prud'homme, J. Cure, V. Constantoudis, G. Papavieros, S. Roualdes, C. Vahlas, TiO2 nanotree films for the production of green H_2 by solar water splitting: From microstructural and optical characteristics to the photocatalytic properties, Appl. Surf. Sci. 494 (2019) 1127–1137, https://doi.org/10.1016/j.apsusc.2019.07.191.

[5] M. Terracciano, V. Galstyan, I. Rea, M. Casalino, L. De Stefano, G. Sbervegleri, Chemical modification of TiO_2 nanotube arrays for label-free optical biosensing applications, Appl. Surf. Sci. 419 (2017) 235–240, https://doi.org/10.1016/j.apsusc.2017.05.029.

[6] X. Li, Y. Zhang, T. Li, Q. Zhong, H. Li, J. Huang, Graphene nanoscrolls encapsulated TiO_2 (B) nanowires for lithium storage, J. Power Sources 268 (2014) 372–378, https://doi.org/10.1016/j.jpowsour.2014.06.056.

[7] J. Wang, R. Ran, M.O. Tade, Z. Shao, Self-assembled mesoporous TiO2/carbon nanotube composite with a three-dimensional conducting nanonetwork as a high-rate anode material for lithium-ion battery, J. Power Sources 254 (2014) 18–28, https://doi.org/10.1016/j.jpowsour.2013.12.090.

[8] A. Meng, L. Zhang, B. Cheng, J. Yu, Dual cocatalysts in TiO2 photocatalysis, Adv. Mater. (2019) 1807660 (1)-(30). https://doi.org/10.1002/adma.201807660.

[9] S. Banerjee, D.D. Dionysiou, S.C. Pillai, Self-cleaning applications of TiO_2 by photo-induced hydrophilicity and photocatalysis, Appl. Catal. B 176-177 (2015) 396–428, https://doi.org/10.1016/j.apcatb.2015.03.058.

[10] K. Liu, M. Cao, A. Fujishima, L. Jiang, Bio-inspired titanium dioxide materials with special wettability and their applications, Chem. Rev. 114 (19) (2014) 10044–10094, https://doi.org/10.1021/cr4006796.

[11] W.J. Lo, Y.W. Chung, G.A. Somorjai, Electron spectroscopy studies of the chemisorption of O_2, H_2 and H_2O on the TiO_2 (100) surfaces with varied stoichiometry: Evidence for the photogeneration of Ti^{+3} and for its importance in chemisorption, Surf. Sci. 71 (1978) 199–219, https://doi.org/10.1016/0039-6028(78)90328-X.

[12] J.G. Highfield, M. Graetzel, Discovery of reversible photochromism in titanium dioxide using photoacoustic spectroscopy: implications for the investigation of light-induced charge-separation and surface redox processes in titanium dioxide, J. Phys. Chem. 92 (2) (1988) 464–467, https://doi.org/10.1021/j100313a043.

[13] R. Wang, N. Sakai, A. Fujishima, T. Watanabe, K. Hashimoto, Studies of surface wettability conversion on TiO2 single-crystal surfaces, J. Phys. Chem. B 103 (12) (1999) 2188–2194, https://doi.org/10.1021/jp983386x.

[14] Y. Li, B. Xia, B. Jiang, Thermal-induced durable superhydrophilicity of TiO2 films with ultra-smooth surfaces, J. Sol-Gel Sci. Technol. 87 (2018) 50–58, https://doi.org/10.1007/s10971-018-4684-0.

[15] K. Nakata, A. Fujishima, TiO_2 photocatalysis: Design and applications, J. Photochem. Photobiol., C 13 (3) (2012) 169–189, https://doi.org/10.1016/j.jphotochemrev.2012.06.001.

[16] R. Wang, K. Hashimoto, A. Fujishima, M. Chikuni, E. Kojima, A. Kitamura, M. Shimohigoshi, T. Watanabe, Photogeneration of highly amphiphilic TiO_2 surfaces, Adv. Mater. 10 (1998) 135–138, https://doi.org/10.1002/(SICI)1521-4095(199801)10:2<135::AID-ADMA135>3.0.CO;2-M.

[17] T. Adachi, S.S. Latthe, S.W. Gosavi, N. Roy, N. Suzuki, H. Ikari, K. Kato, K.-I. Katsumata, K. Nakata, M. Furudate, T. Inoue, T. Kondo, M. Yuasa, A. Fujishima, C. Terashima, Photocatalytic, superhydrophilic, self-cleaning TiO_2 coating on cheap, light-weight, flexible polycarbonate substrates, Appl. Surf. Sci. 458 (2018) 917–923, https://doi.org/10.1016/j.apsusc.2018.07.172.

[18] S. Permpoon, M. Houmard, D. Riassetto, L. Rapenne, G. Berthomé, B. Baroux, J.C. Joud, M. Langlet, Natural and persistent superhydrophilicity of SiO_2/TiO_2 and TiO_2/SiO_2 bi-layer films, Thin Solid Films 516 (6) (2008) 957–966, https://doi.org/10.1016/j.tsf.2007.06.005.

[19] A. Borras, A. Barranco, A.R. González-Elipe, Reversible superhydrophobic to superhydrophilic conversion of Ag@TiO 2 composite nanofiber surfaces, Langmuir 24 (15) (2008) 8021–8026, https://doi.org/10.1021/la800113n.

[20] Z. Duan, Y.u. Zhu, P. Ren, J. Jia, S. Yang, G. Zhao, Y. Xie, J. Zhang, Non-UV activated superhydrophilicity of patterned Fe-doped TiO_2 film for anti-fogging and photocatalysis, Appl. Surf. Sci. 452 (2018) 165–173, https://doi.org/10.1016/j.apsusc.2018.05.029.

[21] C. Garlisi, C.-Y. Lai, L. George, M. Chiesa, G. Palmisano, Relating photoelectrochemistry and wettability of sputtered Cu- and N-Doped TiO 2 thin films via an integrated approach, J. Phys. Chem. C 122 (23) (2018) 12369–12376, https://doi.org/10.1021/acs.jpcc.8b03650.

[22] M. Houmard, D. Riassetto, F. Roussel, A. Bourgeois, G. Berthomé, J.C. Joud, M. Langlet, Enhanced persistence of natural super-hydrophilicity in TiO_2–SiO_2 composite thin films deposited via a sol–gel route, Surf. Sci. 602 (21) (2008)

3364–3374, https://doi.org/10.1016/j.susc.2008.09.016.
[23] M. Houmard, G. Berthomé, J.C. Joud, M. Langlet, Enhanced cleanability of superhydrophilic TiO_2–SiO_2 composite surfaces prepared via a sol–gel route, Surf. Sci. 605 (3-4) (2011) 456–462, https://doi.org/10.1016/j.susc.2010.11.017.
[24] S. Anandan, T. Narasinga Rao, M. Sathish, D. Rangappa, I. Honma, M. Miyauchi, Superhydrophilic graphene-loaded TiO2 thin film for self-cleaning applications, ACS Appl. Mater. Interfaces 5 (1) (2013) 207–212, https://doi.org/10.1021/am302557z.
[25] J. Zhu, Y. Cao, J. He, Facile fabrication of transparent, broadband photoresponse, self-cleaning multifunctional graphene–TiO_2 hybrid films, J. Colloid Interface Sci. 420 (2014) 119–126, https://doi.org/10.1016/j.jcis.2014.01.015.
[26] S. Prabhu, L. Cindrella, O. Joong Kwon, K. Mohanraju, Superhydrophilic and self-cleaning rGO-TiO 2 composite coatings for indoor and outdoor photovoltaic applications, Sol. Energy Mater. Sol. Cells 169 (2017) 304–312, https://doi.org/10.1016/j.solmat.2017.05.023.
[27] Y. Zhang, F. Fu, F. Zhou, X. Yang, D. Zhang, Y. Chen, Synergistic effect of RGO/TiO_2 nanosheets with exposed (001) facets for boosting visible light photocatalytic activity, Appl. Surf. Sci. 510 (2020) 145451, , https://doi.org/10.1016/j.apsusc.2020.145451.
[28] F. Xu, P. Na, String and ball-like TiO2/rGO composites with high photo-catalysis degradation capability for methylene blue, Trans. Tianjin Univ. 24 (3) (2018) 272–281, https://doi.org/10.1007/s12209-018-0119-9.
[29] R. Liu, W. Guo, B. Sun, J. Pang, M. Pei, G. Zhou, Composites of rutile TiO_2 nanorods loaded on graphene oxide nanosheet with enhanced electrochemical performance, Electrochim. Acta 156 (2015) 274–282, https://doi.org/10.1016/j.electacta.2015.01.012.
[30] B.S. Gonçalves, H.G. Palhares, T.C.C. de Souza, V.G. de Castro, G.G. Silva, B.C. Silva, K. Krambrock, R.B. Soares, V.F.C. Lins, M. Houmard, E.H.M. Nunes, Effect of the carbon loading on the structural and photocatalytic properties of reduced graphene oxide-TiO_2 nanocomposites prepared by hydrothermal synthesis, J. Mater. Res. Technol. 8 (6) (2019) 6262–6274, https://doi.org/10.1016/j.jmrt.2019.10.020.
[31] B.S. Gonçalves, L.M.C. Silva, T.C.C. de Souza, V.G. de Castro, G.G. Silva, B.C. Silva, K. Krambrock, R.B. Soares, V.F.C. Lins, M. Houmard, E.H.M. Nunes, Solvent effect on the structure and photocatalytic behavior of TiO 2 -RGO nanocomposites, J. Mater. Res. 34 (23) (2019) 3918–3930, https://doi.org/10.1557/jmr.2019.342.
[32] M. Houmard, D. Riassetto, F. Roussel, A. Bourgeois, G. Berthomé, J.C. Joud, M. Langlet, Morphology and natural wettability properties of sol–gel derived TiO_2–SiO_2 composite thin films, Appl. Surf. Sci. 254 (5) (2007) 1405–1414, https://doi.org/10.1016/j.apsusc.2007.06.072.
[33] M. Houmard, E.H.M. Nunes, D.C.L. Vasconcelos, G. Berthomé, J.-C. Joud, M. Langlet, W.L. Vasconcelos, Correlation between sol–gel reactivity and wettability of silica films deposited on stainless steel, Appl. Surf. Sci. 289 (2014) 218–223, https://doi.org/10.1016/j.apsusc.2013.10.137.
[34] V.G. Castro, J.C. Neves, N.M. Pereira, A.L.S. Assis, L.A. Montoro, G.G. Silva, Process for obtaining graphite oxide and graphene oxide: Products and uses, BR 102016005632-2 A2 (2017).
[35] M. Langlet, A. Kim, M. Audier, C. Guillard, J.M. Herrmann, Liquid phase processing and thin film deposition of titania nanocrystallites for photocatalytic applications on thermally sensitive substrates, J. Mater. Sci. 38 (2003) 3945–3953, https://doi.org/10.1023/A:1026150213468.
[36] R. López, R. Gómez, Band-gap energy estimation from diffuse reflectance measurements on sol–gel and commercial TiO_2: a comparative study, J. Sol-Gel Sci. Technol. 61 (1) (2012) 1–7, https://doi.org/10.1007/s10971-011-2582-9.
[37] E.M. Girotto, I.A. Santos, Medidas de resistividade elétrica DC em sólidos: Como efetuá-las corretamente, Quim. Nova. 25 (2002) 639–647, https://doi.org/10.1590/s0100-40422002000400019 (in Portuguese).
[38] P. Song, X. Zhang, M. Sun, X. Cui, Y. Lin, Graphene oxide modified TiO_2 nanotube arrays: enhanced visible light photoelectrochemical properties, Nanoscale 4 (5) (2012) 1800, https://doi.org/10.1039/c2nr11938b.
[39] M.M. Lucchese, F. Stavale, E.H.M. Ferreira, C. Vilani, M.V.O. Moutinho, R.B. Capaz, C.A. Achete, A. Jorio, Quantifying ion-induced defects and Raman relaxation length in graphene, Carbon 48 (5) (2010) 1592–1597, https://doi.org/10.1016/j.carbon.2009.12.057.
[40] Y. Zhang, N. Zhang, Z.-R. Tang, Y.-J. Xu, Improving the photocatalytic performance of graphene–TiO_2 nanocomposites via a combined strategy of decreasing defects of graphene and increasing interfacial contact, Phys. Chem. Chem. Phys. 14 (25) (2012) 9167–9175, https://doi.org/10.1039/c2cp41318c.
[41] T. Xing, L.H. Li, L. Hou, X. Hu, S. Zhou, R. Peter, M. Petravic, Y. Chen, Disorder in ball-milled graphite revealed by Raman spectroscopy, Carbon 57 (2013) 515–519, https://doi.org/10.1016/j.carbon.2013.02.029.
[42] Y.H. Ding, P. Zhang, Q. Zhuo, H.M. Ren, Z.M. Yang, Y. Jiang, A green approach to the synthesis of reduced graphene oxide nanosheets under UV irradiation, Nanotechnology 22 (21) (2011) 215601, https://doi.org/10.1088/0957-4484/22/21/215601.
[43] O. Akhavan, M. Abdolahad, A. Esfandiar, M. Mohatashamifar, Photodegradation of Graphene Oxide Sheets by TiO 2 Nanoparticles after a Photocatalytic Reduction, J. Phys. Chem. C 114 (30) (2010) 12955–12959, https://doi.org/10.1021/jp103472c.
[44] M.H.M. Zaid, K.A. Matori, S.H. Abdul Aziz, A. Zakaria, M.S.M. Ghazali, Effect of ZnO on the physical properties and optical band gap of soda lime silicate glass, Int. J. Mol. Sci. 13 (2012) 7550–7558. https://doi.org/10.3390/ijms13067550.
[45] L.E. Scriven, Physics and applications of dip coating and spin coating, MRS Proc. 121 (1988) 717–729, https://doi.org/10.1557/proc-121-717.
[46] Y. Zhang, Q. Shen, J. Hou, P.D. Sutrisna, V. Chen, Shear-aligned graphene oxide laminate/Pebax ultrathin composite hollow fiber membranes using a facile dip-coating approach, J. Mater. Chem. A 5 (17) (2017) 7732–7737, https://doi.org/10.1039/c6ta10395b.
[47] A.C. Pedreira de Freitas, L.C. Espejo, S.B. Botta, F.d.S. Teixeira, M.A.A.C. Luz, N. Garone-Netto, A.B. Matos, M.C.B.d.S. Salvadori, AFM analysis of bleaching effects on dental enamel microtopography, Appl. Surf. Sci. 256 (9) (2010) 2915–2919, https://doi.org/10.1016/j.apsusc.2009.11.050.
[48] H. Zhang, X. Lv, Y. Li, Y. Wang, J. Li, P25-Graphene Composite as a High Performance Photocatalyst, ACS Nano 4 (1) (2010) 380–386, https://doi.org/10.1021/nn901221k.
[49] J.-G. Lee, D.-Y. Kim, J.-J. Park, Y.-H. Cha, J.Y. Yoon, H.S. Jeon, B.K. Min, M.T. Swihart, S. Jin, S.S. Al-Deyab, S.S. Yoon, R.-J. XIE, Graphene-Titania Hybrid Photoanodes by Supersonic Kinetic Spraying for Solar Water Splitting, J. Am. Ceram. Soc. 97 (11) (2014) 3660–3668, https://doi.org/10.1111/jace.13174.
[50] H.J. Busscher, A.W.J. van Pelt, P. de Boer, H.P. de Jong, J. Arends, The effect of surface roughening of polymers on measured contact angles of liquids, Colloids Surf. 9 (4) (1984) 319–331, https://doi.org/10.1016/0166-6622(84)80175-4.
[51] P.F. Wang, Z.H. Li, Y.M. Zhu, Research on the direct doping effect of silicon on cubic boron nitride ceramics by UV–VIS diffuse reflectance, Mater. Chem. Phys. 123 (2-3) (2010) 356–359, https://doi.org/10.1016/j.matchemphys.2010.05.050.
[52] M. Schiavello, Heterogeneous Photocatalysis (Wiley Series in Photoscience & Photoengineering), New York, NY, 1997.
[53] K. Madhusudan Reddy, S.V. Manorama, A. Ramachandra Reddy, Bandgap studies on anatase titanium dioxide nanoparticles, Mater. Chem. Phys. 78 (1) (2003) 239–245, https://doi.org/10.1016/S0254-0584(02)00343-7.
[54] J. Zhang, P. Zhou, J. Liu, J. Yu, New understanding of the difference of photocatalytic activity among anatase, rutile and brookite TiO 2, Phys. Chem. Chem. Phys. 16 (38) (2014) 20382–20386, https://doi.org/10.1039/c4cp02201g.
[55] G. Williams, B. Seger, P.V. Kamat, TiO 2 -Graphene Nanocomposites. UV-Assisted Photocatalytic Reduction of Graphene Oxide, ACS Nano 2 (7) (2008) 1487–1491, https://doi.org/10.1021/nn800251f.
[56] N. Sakai, K. Kamanaka, T. Sasaki, Modulation of Photochemical Activity of Titania Nanosheets via Heteroassembly with Reduced Graphene Oxide. Enhancement of Photoinduced Hydrophilic Conversion Properties, J. Phys. Chem. C 120 (42) (2016) 23944–23950, https://doi.org/10.1021/acs.jpcc.6b06842.
[57] K.-Y. Lian, Y.-F. Ji, X.-F. Li, M.-X. Jin, D.-J. Ding, Y.i. Luo, Big Bandgap in Highly Reduced Graphene Oxides, J. Phys. Chem. C 117 (12) (2013) 6049–6054, https://doi.org/10.1021/jp3118067.
[58] Y. Chen, H. Gao, J. Xiang, X. Dong, Y. Cao, Enhanced photocatalytic activities of TiO2-reduced graphene oxide nanocomposites controlled by Ti O C interfacial chemical bond, Mater. Res. Bull. 99 (2018) 29–36, https://doi.org/10.1016/j.materresbull.2017.08.054.
[59] A. Fujishima, K. Honda, Electrochemical photolysis of water at a semiconductor electrode, Nature 238 (1972) 37–38, https://doi.org/10.1038/238037a0.
[60] A.B. Héctor, M. Jie, L. Zunfeng, B. Randall, M. Stoltenberg Zhenan, C. Yongsheng, H.A. Becerril, J. Mao, Z. Liu, R.M. Stoltenberg, Z. Bao, Y. Chen, Evaluation of solution-processed reduced graphene oxide films as as transparent conductors, ACS Nano 2 (2008) 463–470, https://doi.org/10.1021/nn700375n.
[61] Z. Yin, S. Sun, T. Salim, S. Wu, X. Huang, Q. He, Y.M. Lam, H. Zhang, Organic Photovoltaic Devices Using Highly Flexible Reduced Graphene Oxide Films as Transparent Electrodes, ACS Nano 4 (9) (2010) 5263–5268, https://doi.org/10.1021/nn1015874.
[62] S.J. Wang, Y. Geng, Q. Zheng, J.-K. Kim, Fabrication of highly conducting and transparent graphene films, Carbon 48 (6) (2010) 1815–1823, https://doi.org/10.1016/j.carbon.2010.01.027.
[63] J.-H. Huang, J.-H. Fang, C.-C. Liu, C.-W. Chu, Effective Work Function Modulation of Graphene/Carbon Nanotube Composite Films As Transparent Cathodes for Organic Optoelectronics, ACS Nano 5 (8) (2011) 6262–6271, https://doi.org/10.1021/nn201253w.
[64] Y.T. Park, A.Y. Ham, J.C. Grunlan, Heating and acid doping thin film carbon nanotube assemblies for high transparency and low sheet resistance, J. Mater. Chem. 21 (2) (2011) 363–368, https://doi.org/10.1039/c0jm02524k.
[65] S. Veltri, A.M. Palermo, G. De Filpo, F. Xu, Subsurface treatment of TiO_2 nanoparticles for limestone: Prolonged surface photocatalytic biocidal activities, Build. Environ. 149 (2019) 655–661, https://doi.org/10.1016/j.buildenv.2018.10.038.
[66] A. Barmeh, M.R. Nilforoushan, S. Otroj, Wetting and photocatalytic properties of Ni-doped TiO_2 coating on glazed ceramic tiles under visible light, Thin Solid Films 666 (2018) 137–142, https://doi.org/10.1016/j.tsf.2018.09.007.
[67] J. Rafiee, M.A. Rafiee, Z.-Z. Yu, N. Koratkar, Superhydrophobic to Superhydrophilic Wetting Control in Graphene Films, Adv. Mater. 22 (19) (2010) 2151–2154, https://doi.org/10.1002/adma.200903696.
[68] J.N. Israelachvili, M.L. Gee, Contact angles on chemically heterogeneous surfaces, Langmuir 5 (1) (1989) 288–289, https://doi.org/10.1021/la00085a059.
[69] P.S. Foran, C. Boxall, K.R. Denison, Photoinduced Superhydrophilicity: A Kinetic Study of Time Dependent Photoinduced Contact Angle Changes on TiO 2 Surfaces, Langmuir 28 (51) (2012) 17647–17655, https://doi.org/10.1021/la3026649.
[70] F. Wang, K. Zhang, Reduced graphene oxide–TiO2 nanocomposite with high photocatalystic activity for the degradation of rhodamine B, J. Mol. Catal. A: Chem. 345 (1-2) (2011) 101–107, https://doi.org/10.1016/j.molcata.2011.05.026.
[71] X. Chen, D. Meng, B. Wang, B.-W. Li, W. Li, C.W. Bielawski, R.S. Ruoff, Rapid thermal decomposition of confined graphene oxide films in air, Carbon 101 (2016) 71–76, https://doi.org/10.1016/j.carbon.2016.01.075.
[72] M. Ghiyasvand, M. Naser-Moghadasi, A.A. Lotfi-Neyestank, A. Nikfarjam, Shielding effectiveness improvement of non-metallic transparent enclosures using gold nanolayer deposition, Appl. Comput. Electromagn. Soc. J. 32 (2017) 1098–1104.
[73] S.L. Gras, T. Mahmud, G. Rosengarten, A. Mitchell, K. Kalantar-zadeh, Intelligent Control of Surface Hydrophobicity, ChemPhysChem 8 (14) (2007) 2036–2050, https://doi.org/10.1002/cphc.200700222.
[74] F. Xia, Y. Zhu, L. Feng, L. Jiang, Smart responsive surfaces switching reversibly between super-hydrophobicity and super-hydrophilicity, Soft Matter 5 (2) (2009) 275–281, https://doi.org/10.1039/b803951h.